Characterization of the Reaction Products of Laser-Ablated Early Lanthanide Metal Atoms with Molecular Oxygen. Infrared Spectra of LnO, LnO^+, LnO^-, LnO_2, LnO_2^+, LnO_2^-, LnO_3^-, and $(LnO)_2$ in Solid Argon

Stephen P. Willson and Lester Andrews*

Chemistry Department, University of Virginia, Charlottesville, Virginia 22901

Received: January 4, 1999; In Final Form: March 2, 1999

This paper is the first of a two-part study of the reaction products of laser-ablated lanthanide metal atoms with O_2. There is general agreement with previous gas-phase and matrix-isolated neutral monoxides of the lanthanide elements. The present results agree with earlier identifications of CeO_2 and PrO_2 and make new assignments for NdO_2, SmO_2, EuO_2, and GdO_2. In addition, this work provides vibrational frequencies for six LnO^+, five LnO^-, two LnO_2^+, six LnO_2^-, and two LnO_3^- species; five $(LnO)_2$ rings are also reported here for the first time. Low ionization energies for the metals and the LnO molecules facilitate production of the LnO^+ cations and make electrons available for capture to form molecular anions. The doping of CCl_4 into these samples provides a diagnostic test for the identification of molecular cations and anions by matrix infrared spectroscopy.

Introduction

The chemistry of the lanthanide elements occupies a prominent position in many branches of chemical research. There is an abundance of biological chemistry dealing with the activity of lanthanides.[1,2] Lanthanide compounds are useful for organic synthesis and catalytic polymerization.[3−5] Most solid-state lasers utilize lanthanide ions, primarily neodymium(III), and there is some potential for lanthanide-based superconductors.[6,7]

Extensive gas-phase literature is available pertaining to most of the neutral lanthanide monoxides,[8−19] with the exception of TmO, for which only matrix-isolated samples have been studied.[20−23] For these molecules, it is common to find many low-lying electronic states, which complicates the spectra considerably. Identification of the ground electronic state is not generally straightforward, but nevertheless, assignments have been made for the gas-phase vibrational fundamental frequencies, which agree well with the previous matrix assignments and place the vibrational fundamentals of all of the lanthanide monoxides in the 820−850 cm^{-1} range, excluding EuO and YbO, which fall between 680 and 690 cm^{-1}. Several theoretical studies of the lanthanide monoxides have also been undertaken in recent years.[24−29]

In addition to the neutral monoxides of the lanthanide metals, there have been a few neutral dioxides identified in matrix isolation experiments[20,21,23] and mass spectrometry observations of monoxide and dioxide cations.[30−33] A recent study of chemiionization reactions and chemielectron spectroscopy of gas-phase lanthanide metals with oxidants has established that CeO^+, PrO^+, NdO^+, SmO^+, GdO^+ and $OCeO^+$ and $OPrO^+$ form spontaneously upon metal atom reaction with molecular oxygen and has postulated that TbO^+, DyO^+, HoO^+, ErO^+, and perhaps LuO^+ do the same.[34] The ozonides of samarium and praseodymium have also been previously identified,[35] in accord with earlier studies with alkali metal atoms.[36] There is a large body of both experimental and theoretical literature available regarding the bulk phase lanthanide oxides.[37−40]

This work agrees with previous identification of the monoxides of the lanthanide elements in both matrix and gas-phase studies.[8−23] In addition, vibrational fundamentals of matrix-isolated monoxide ions are reported, with cations identified for all of the monoxides and anions identified for five of those included in the first half of this study. The vibrational fundamentals of the matrix-isolated neutral dioxide molecules for the first half of the lanthanide series, except PmO_2, are also reported here. The frequencies for CeO_2 and PrO_2 previously reported[21] are confirmed in this study. The NdO_2 fundamental is reported here for the first time and is of interest for comparison to the isoelectronic UO_2 molecule.[41,42] Six dioxide anions and two dioxide cations are identified in this study, as are fundamentals of the $(LnO)_2$ ring species.

Experimental Section

Lanthanide atoms supplied by laser vaporization of metal targets were reacted with molecular oxygen in argon matrices using techniques described in previous publications.[43−46] Experiments required O_2/Ar concentrations ranging from 0.5 to 3% deposited at a rate of 4−5 mmol/h for 1−3 h onto a CsI window held at 6−7 or 10−11 K. Samples of $^{18}O_2$, mixed $^{16}O_2 + {}^{18}O_2$, and scrambled $^{16}O_2 + {}^{16}O^{18}O + {}^{18}O_2$ were also employed. To identify charged products, some gas sample mixtures were doped with CCl_4, not exceeding 10% of the total O_2 concentration in the sample. Complementary neon experiments were done for Pr and Nd with concentrations of 0.2−0.5% O_2 deposited at 4 or 6−7 K. Infrared spectra were recorded at 0.5 cm^{-1} resolution and ±0.1 cm^{-1} accuracy with a Nicolet 750, 550, or 60SXR spectrometer after deposition and after each annealing or photolysis.

The metal targets, Ce (99.99%), Pr, Nd, Sm, Eu, Gd (all Johnson-Matthey 99.9%), were ablated with the 1064 nm fundamental of a YAG laser, typically with 5−50 mJ pulses. For low laser power experiments, a 10% transmitting neutral density filter was placed in the laser beam. Following deposition, argon matrices were annealed to 25 K, then subjected to UV photolysis using a 175 W mercury street lamp (Philips H39KB) without the globe (240−580 nm). Alternately, matrices were subjected to a series of photolyses beginning with a tungsten

10.1021/jp990005m CCC: $18.00
Published on Web 04/13/1999

TABLE 1: Product Absorptions (cm^{-1}) Observed for Laser-Ablated Ce Atoms with O_2 in Solid Argon at 10 K

$^{16}O_2$	$^{18}O_2$	$^{16}O_2 + {}^{18}O_2$	$^{16}O_2 + {}^{16}O{}^{18}O + {}^{18}O_2$	$R(16/18)^a$	anneal[b]	identity
1554.2	1467.1	1554.9, 1467.2	1553.9, 1511.8, 1467.6	1.0594	b+	$(OO)Ce_x$
1489.5	1413.2	1489.3, 1413.2		1.0540	a+ −(+)	CeO_2, $\nu_1 + \nu_3$
1388.3	1379.2	1388.3, 1379.1		1.0066	a− −	HO_2
1369.0	1298.5			1.0543	a+ − (+)	CeO_2^-, $\nu_1 + \nu_3$
1126	1063	1127, 1062	1128, 1097, 1064	1.0596	b+	$(O_2)CeO_2$
1118.6	1055.8	1118.4, 1084.6, 1056.2	1118.7, 1102.6, 1087.9, 1084.9, 1071.2, 1056.4	1.0595	a− − − (−)	O_4^+
1109.0	1046.8	1109.1, 1046.8	1109.1, 1078.8, 1046.8	1.0594	a+0(−)	$(O_2)CeO_2$
1039.6	982.3	1039.4, 1025.4, 991.5, 982.2	1039.4, 1025.4, 1016.5, 1005.9, 991.4, 982.1	1.0583	a+ −(−)	O_3
1033.1	976.2	1033.0, 1019.4, 985.5, 976.2	1032.9, 1019.3, 1010.3, 999.6, 985.4, 976.1	1.0583	a− −(−)	O_3
953.7	901.6	953.6, 924.7, 901.6	953.7, 940.2, 928.1, 924.8, 914.1, 901.7	1.0578	a− −(−)	O_4^-
849.4	805.8	849.5, 805.9	849.6, 805.9	1.0541	a+ −*	CeO^+
823.7	778.6	824, 779		1.0579	a++(−)	$Ce(O_2)$
808.3	767.1	808.4, 767.2	808.4, 767.2	1.0537	a− −(−)*	CeO
804.7	763.7			1.0537	b+	$(O_2)_xCeO$
804.1	759.2			1.0591	a− −(−)	O_3^-
772.8	733.8			1.0531	a+ −**	CeO^-
757.3	715.6	757.3, 715.7	757.2, 749.0, 715.6	1.0583	a+ −(+)	CeO_2, ν_1
736.7	701.7	736.9, 701.8	736.9, 707.1, 701.8	1.0499	a− − (+)	CeO_2, ν_3
731.9	697.0	731.9, 697.0	731.8, - - -, 697.0	1.0501	b+	$(O_2)CeO_2$
718.7	681.5			1.0546	a+ −(−)	?
712.0	672.9	711.9, 673.0	- - -, - - -, 673.0	1.0581	a+ −(+)**	CeO_2^-, ν_1
662.0	630.6	661.9, 630.6	661.9, 640.4, 630.6	1.0498	a+ −(+)**	CeO_2^-, ν_3
575.0	547.1	575.2, 561.5, 547.5	574.9, 561.5, 547.7	1.0510	a+ −(+)	$(CeO)_2$
483.6	459.5	483.7, 470.1, 459.7	483.6, 470.1, 459.6	1.0524	a+ −(+)	$(CeO)_2$

[a] Ratio (16/18) of isotopic frequencies, based on 0.1 cm^{-1} frequency accuracy. These ratios are accurate to better than ±0.0004. [b] Annealing behavior: a denotes presence on deposition and +, −, or 0 indicates the direction of growth in two successive annealings; b denotes appearance on the first annealing and +, −, or 0 indicates changes on second annealing; (+ or −) indicates changes on photolysis; * indicates an increase with CCl_4 on deposition; ** indicates a decrease with CCl_4 on deposition.

lamp, with glass filters, and finally with the mercury arc lamp. An annealing cycle consists of raising the matrix temperature to the specified value, then cooling back to the deposition temperature. Further annealings were done after photolysis, and additional spectra were recorded.

Several experiments were also done using a pulsed valve at a rate of 10 Hz to deposit reactant gas samples in sync with laser ablation of the metal target. The gas outlet was positioned a few centimeters from the cold substrate beside the target, with both directed at the CsI window, and the valve remained open for about 8 ms with the laser firing in the first third of that time span. Backing pressures of the valve ranged from subatmospheric to 100 psig. An additional experiment was done gating molecular O_2 only through the pulsed valve, depositing the O_2 and metal atoms into a continuous stream of argon from a separate nozzle.

Results

Absorptions observed for the laser-ablated lanthanide metal atom + dioxygen reaction systems fall into two broad categories, those identified as O−O vibrations and those due to Ln−O motions. Oxygen−oxygen vibrations observed range from a perturbed O_2 vibration near 1552 cm^{-1} to the O_3^- fundamental at 804 cm^{-1} in solid argon and include O_4^+ at 1118.6, O_3 at 1039.6 and 1033.1, and O_4^- at 953.7 cm^{-1},[47−51] which are found for all metals but only listed in Table 1. The metal−oxygen fundamentals range from 400 to 1000 cm^{-1}, and absorption bands for each metal are listed with their $^{18}O_2$ isotopic counterparts and annealing behavior in Tables 1−6; differences observed after photolysis or with the doping of samples with CCl_4 are also included with the annealing data. For Pr and Nd, neon results are listed below the argon results in the same table. Examples of important spectral regions are provided in Figures 1−6 for clarification of the text.

The results of the pulsed valve experiments were similar to those of the standard continuous flow experiments and so are not separated from the greater body of work. Although this method produced comparable concentrations of products in a shorter period of time, no new products were observed, and the advantages were not significant enough to warrant alteration of the standard experiment.

Discussion

The primary reaction products of laser-ablated lanthanide metal atoms with molecular O_2 are LnO, LnO_2, and $(LnO)_2$. The ablated metal atoms form energized dioxide insertion products, which are relaxed by the matrix or decomposed to the monoxide molecules:

$$Ln + O_2 \rightarrow [OLnO]^* \rightarrow LnO_2 \text{ or } O + LnO \qquad (1)$$

The monoxides and dioxides have also been observed in cationic, neutral, and anionic states. Determination of the charge on a given metal oxide is based on results obtained from doping reactant gas mixtures with CCl_4 to capture electrons, thereby minimizing the formation of metal oxide anions and favoring cations. This technique has successfully supported the identification of MCO^+ and MCO^-, CO_2^+ and CO_2^-, and $C_2O_4^+$ and $C_2O_4^-$ species as confirmed by DFT calculations.[52−56] Identification of the neutral molecules agrees with previous thermal matrix isolation and gas-phase assignments for all of the lanthanide monoxides and two of the dioxides.[8−23] In the current study, it has been discovered that cations of the lanthanide monoxides and dioxides absorb at higher frequencies than the neutral, while anions absorb at lower frequencies, as is expected from a simple ionic model. Increasing the charge on the metal center strengthens the bond to O, and conversely, decreasing the metal charge weakens the attraction. The discussion is divided into sections based on molecular formula, with the ions of each metal analogue discussed in turn and oxygen-16 frequencies provided with oxygen-18 counterparts in parentheses.

Monoxides. All lanthanide oxide systems provided neutral monoxides and singly charged monoxide cations, and five

produced singly charged anions. Identification of monoxide species is dependent both on the isotopic frequency ratio and on the number of corresponding peaks in isotopically scrambled oxygen samples. Oxygen isotopic ratios are in close agreement with the harmonic LnO ratios and the scrambled $^{16}O_2 + {}^{16}O^{18}O + {}^{18}O_2$ samples provide doublets, indicating the motion of exactly one oxygen atom in the observed vibrations. Doping with CCl_4 generally decreased the overall product yield while increasing cation and decreasing anion absorptions relative to neutral molecule absorption intensities, which arises because electrons are effectively trapped by CCl_4.[57] Considering a simple ligand field model, it is not surprising that the LnO^+ ion is so prevalent, as it places a +3 charge on the metal, which is a common oxidation state of all the lanthanides. Furthermore, several of the LnO^+ species form exothermically from the reaction of Ln with O, releasing an electron.[34] Chemiionization reaction 2 is spontaneous for Ln = Ce, Pr, Nd, Sm, and Gd.[34]

$$Ln + O \rightarrow LnO^+ + e^- \quad (2)$$

Direct reaction 3 merits consideration, as metal cations are produced by laser ablation.

$$Ln^+ + O \rightarrow LnO^+ \quad (3)$$

Photoionization reaction 4 is observed in this study for matrix-isolated molecules; ionization energies of the LnO molecules are near 5 eV,[31,34] which is conveniently coincident with the strong mercury arc emission.

$$LnO + h\nu \rightarrow LnO^+ + e^- \quad (4)$$

The LnO^- anions are formed in these experiments by electron capture reaction 5, since the electron affinities of LnO molecules are expected to be in the range of transition metal monoxides (CuO, 1.77 eV; VO, 1.23 eV).[58,59]

$$LnO + e^- \rightarrow LnO^- \quad (5)$$

The LnO^- anion absorptions increase in these experiments upon tungsten lamp photolysis as the O_4^- absorption is destroyed. Since O_4^- can be expected to dissociate (10.5 kcal/mol)[60] to O_2 and O_2^-, and the latter detach (10.1 kcal/mol),[60] near-infrared radiation with energy in excess of 20.6 kcal/mol should provide electrons for capture by LnO molecules.

Vibrational frequencies of molecules and ions trapped in neon are closer to the gas-phase values than those in argon, as is clearly borne out by the PrO molecule, for which the argon value is about 13 cm^{-1} below the gas-phase frequency, while the neon value is only 2 cm^{-1} red-shifted from the gas phase. The matrix shift from an argon to a neon host has been observed in the Pr and Nd systems to be greater for the ions of the monoxide species than for the neutral molecules, supporting the proposition that the argon host has in general a stronger effect on the vibrations of charged species than on neutrals. This is an expected result due to the higher polarizability of argon compared to neon and the greater polarization of the host molecule achieved by exposure to a charged species, as has been observed for a large number of molecules.[61]

CeO Species. The cation, anion, and neutral CeO molecules have been identified in spectra of cerium with O_2 in argon matrices (Figure 1). All exhibit exactly two absorptions both in the mixed $^{16}O_2 + {}^{18}O_2$ and the scrambled $^{16}O_2 + {}^{16}O^{18}O + {}^{18}O_2$ experiments, indicative of the vibration of a single O atom (Table 1). The CeO^+ cation absorbs at 849.4 (805.8) cm^{-1} and was not affected by photolysis in these experiments. The

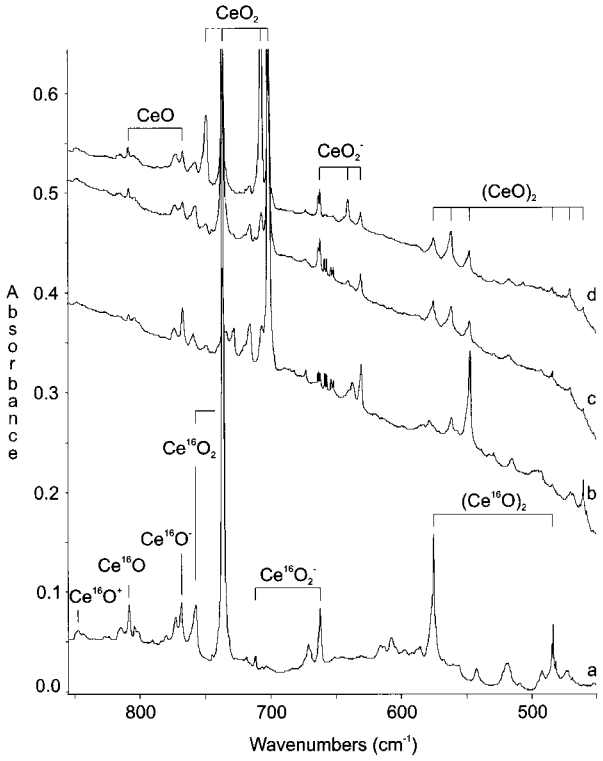

Figure 1. Infrared spectra in the 855−450 cm^{-1} region for laser-ablated cerium atoms co-deposited with (a) 1% $^{16}O_2$/Ar after 50 min deposition, (b) 1% $^{18}O_2$/Ar after 1 h deposition, (c) 2% ($^{16}O_2 + {}^{18}O_2$)/Ar after 50 min deposition, (d) 2% ($^{16}O_2 + {}^{16}O^{18}O + {}^{18}O_2$)/Ar after 50 min deposition.

observed $^{16}O/^{18}O$ isotopic ratio of CeO^+, 1.0541, is identical to the harmonic oscillator ratio. The CeO neutral absorbs at 808.3 (767.1) cm^{-1} and has been previously assigned in matrix work with thermally evaporated cerium oxide.[20] The CeO^- anion fundamental occurs at 768.1 (727.7) cm^{-1} and is reported here for the first time. Introduction of trace CCl_4 to the reaction mixture increases the relative yield of CeO^+ while decreasing CeO^-.

PrO Species. PrO is observed in neutral, positively charged, and negatively charged oxidation states, PrO, PrO^+, and PrO^- (Table 2). The cation absorbs weakly at 857.4 (813.4) cm^{-1} and is stronger in higher laser power experiments. The oxygen isotopic ratio of the cation is 1.0541, in agreement with the harmonic oscillator ratio, and it does not have intermediate isotopic peaks in either mixed or scrambled oxygen samples. The neutral molecule is assigned at 816.7 (775.0) cm^{-1}, in agreement with previous findings[20,21] (Figure 2). The anion absorbs weakly at 767.4 (728.3) cm^{-1} and is not present in higher laser power experiments. Although the anion could not be identified in mixed or scrambled isotopic oxygen experiments due to the much greater intensity of nearby peaks, its oxygen isotopic ratio of 1.0537 is consistent with a diatomic molecule, and its proximity to other lanthanide monoxide anions lends further credence to this assignment. Doping of reactant gas samples with CCl_4 increases the cation intensity while decreasing the neutral and the anion, consistent with the identification of these species.

All three PrO moieties are also observed in neon matrices at 4 K (Figure 3). Comparison of band positions from Table 2 and Figures 2 and 3 demonstrates that the argon matrix to neon matrix blue shift in frequency is greater for PrO^+ and PrO^- than for PrO neutral, about 25 cm^{-1} for both of the former and 11 cm^{-1} for the latter.

TABLE 2: Product Absorptions (cm^{-1}) Observed for Laser-Ablated Pr Atoms with O_2 in Solid Argon and Neon

$^{16}O_2$	$^{18}O_2$	$^{16}O_2 + {}^{18}O_2$	$^{16}O_2 + {}^{16}O^{18}O + {}^{18}O_2$	$R(16/18)$[a]	anneal[b]	identity
			In Argon			
1555.1	1467.7	1555.3, 1467.7		1.0595	b+	$(OO)Pr_x$
1515.5	1438.9	1515.4, 1439.1		1.0532	a++(−)	$(O_2)PrO_2$, $\nu_1 + \nu_3$
1495.6	1420.3	1495.8, 1420.7	1496.0, 1458.4, 1420.3	1.0530	b+	?
1488.9	1405.9	1489.0, 1406.0	1489.0, 1448.3, 1406.0	1.0590	a0−	?
1424.4	1351.5	1424.4, 1351.6	1424.5, 1390.8, 1351.4	1.0539	a+ −(+)	PrO_2, $\nu_1 + \nu_3$
1422.0	1349.2	1422.0, 1349.2		1.0540	a+ −	PrO_2, $\nu_1 + \nu_3$ site
1416.0	1336.9			1.0592	b−(−)	cyc-O_6^+
1331.5	1261.4	1331.3, 1291.3, 1261.5	1331.4, 1313.0, 1297.2, 1291.5, 1277.9, 1261.5	1.0556	a+ −(−)	$(O_2)_2PrO_2$
1328.8	1259.0	1328.7, 1288.9, 1259.0	1328.8, 1310.5, 1294.6, 1289.0, 1275.4, 1259.3	1.0554	a+ −(−)	$(O_2)_2PrO_2$
1301.9	1235.7	1301.6, 1235.4		1.0536	a− −**	?
1185.9	1118.9	1185.8, 1118.8		1.0599	a+ −(−)	?
1142.7	1078.5	1142.7, 1078.8	1142.9, 1112.0, 1079.0	1.0595	b+	$(O_2)PrO_2$ site
1141.5	1077.3	1141.5, 1077.3	1141.6, 1109.8, 1077.3	1.0596	a++(−)**	$(O_2)PrO_2$
914.1	872.1	914.1, 872.1	914.1, 896.1, 872.1	1.0482	a+ −(−)*	PrO_2^+, ν_3
906.7	865.0	906.8, 865.0		1.0482	b+	$(OO)_xPrO_2^+$, ν_3
891.9	851.0	891.8, 850.9	891.8, 874.4, 850.9	1.0481	b+	$(OO)_xPrO_2^+$, ν_3
857.4	813.4			1.0541	a+ −*	PrO^+
836.8	798.5	836.9, 798.6		1.0480	b+	$(O_2)_2PrO_2$, ν_3
830.3	792.3	830.3, 814.3, 792.4	830.3, 814.2, 792.4	1.0480	b+(−)	$(O_2)_2PrO_2$, ν_3 site
(827)	780.5	(827), 780.5	(827), 804.1, 780.6	1.060	a− −(−)**	$Pr(O_2)$
826.9	789.1	826.9, 789.1	826.9, 810.7, 789.0	1.0479	a++(−)**	$(O_2)PrO_2$, ν_3
823.4	785.7	823.4, 785.8	823.3, 807.4, 785.7	1.0480	b+	$(O_2)PrO_2$, ν_3 site
819.6	777.6	819.7, 777.5	819.6, 777.7	1.0540	a0-**	PrO site
817.4	780.1	817.5, 780.1	817.4, 801.5, 780.1	1.0478	b+	$(O_2)PrO_2$, ν_3 site
816.9	775.2	816.8, 775.1	816.9, 775.2	1.0538	a− −(−)**	PrO
810.7	769.4	810.8, 769.1	810.8, 769.5	1.0537	a− −(−)**	PrO site
797	752	- - -, - - -, 762, 752	- - -, - - -, - - -, 772, 762, 752	1.060	b+(−)	$Pr^+O_3^-$
771.2	736.1	771.2, 736.2	771.1, 756.1, 736.2	1.0477	b+	?
767.4	728.3			1.0537	a0−(−)**	PrO^-
731.8	697.9	731.8, 697.9	731.8, 721.8, 697.9	1.0486	a0−	PrO_2, ν_3 site
730.1	696.1	730.0, 696.1	730.1, 721.1, 696.1	1.0488	a+ −(+)	PrO_2, ν_3
727.4	693.6	727.4, 693.5	727.4, 718.1, 693.4 671.4	1.0487	b−	PrO_2, ν_3 site
					a+ −(+)	PrO_2, ν_1
699.2	663.0	699.4, 663.1		1.0546	a+ −(+)**	$(PrO)_2$
679.1	646.1	680.7, 646.3	680.7, 663.0, 646.3	1.0532	b+	$(OO)_x(PrO)_2$
677.1	642.4			1.0540	a− −(−)**	?
665.0	628.2	664.9, 628.3	664.8, 659.8, 628.2	1.0586	a+ −(−)**	PrO_2^-, ν_1
653.8	623.2	653.8, 623.2	653.8, 625.3, 623.2	1.0491	a+ −(−)**	PrO_2^-, ν_3
646.5	616.3			1.0490	a0−(−)**	PrO_2^-, ν_3 site
605.8, 593.7	568.4, 560.6			1.0658, 1.0590	a+ −(+)**	$(PrO)_2$
596.1	567.0	596.1, 567.1	596.1, 582.7, 567.2	1.0513	b+	$(OO)_x(PrO)_2$
573.9	546.0	573.9, 560.6, 552.6, 546.1	573.7, 560.6, 552.5, 546.0	1.0511	a+ −**	PrO_3^-
467.0	444.8	466.7, 445.0		1.0499	a+ −	?
			In Neon			
1554.5	1466.8			1.0598	a+	$(OO)Pr_x$
1490.1	1409.6			1.0571	a++(−)	?
1462.5	1387.5			1.0541	b+	PrO_2, $\nu_1 + \nu_3$
1457.4	1382.5			1.0542	a−(+)	PrO_2, $\nu_1 + \nu_3$ site
1448.3	1374.1			1.0540	b+(−)	PrO_2, $\nu_1 + \nu_3$ site
1429.3	1349.5			1.0591	a++(−)	trans-O_6^+
1320.1	1251.9			1.0545	a++(−)	cyc-O_4^+
1164.1	1098.6			1.0596	a++(−)	trans-O_4^+
1143.0	1078.7			1.0596	b+	$(O_2)PrO_2$
1140.3	1076.1			1.0597	b+	$(O_2)PrO_2$ site
1039.7	982.6			1.0581	a++(−)	O_3
1038.4	981.3			1.0582	a++(−)	O_3
1009.1	954.0			1.0578	a+0(−)	?
972.9	919.5			1.0581	a− −(−)	cyc-O_4^-
967.5	914.3			1.0582	a− −(−)	cyc-O_4^- site
939.8	896.6			1.0482	a+ −(+)	PrO_2^+, ν_3
933.8	890.9			1.0482	b+(−)	PrO_2^+, ν_3 site
928.3	885.6			1.0482	b+(−)	PrO_2^+, ν_3 site
882.3	837.2			1.0539	a0+(−)	PrO^+
878.7	833.8			1.0538	b+(−)	PrO^+ site
841.4	802.9			1.0480	a++(−)	$(O_2)PrO_2$, ν_3
834.3	796.1			1.0480	b+	$(O_2)PrO_2$, ν_3 site
828.0	785.7			1.0538	a− −(−)	PrO
792.6	751.8			1.0543	a0−	PrO^-
752.5	717.5			1.0488	a+ −(+)	PrO_2, ν_3
749.0	714.4			1.0484	a++(+)	PrO_2, ν_3 site
746.3	711.6			1.0488	b0	PrO_2, ν_3 site
713	677			1.053	a0−(+)	$(PrO)_2$
667.6	636.2			1.0494	a0−(−)	PrO_2^-, ν_3
664.5	633.3			1.0493	a0−(−)	PrO_2^-, ν_3 site
662.4	631.3			1.0493	a0−(−)	PrO_2^-, ν_3 site
585.3	557.2			1.0504	a0−(−)	PrO_3^-

[a] Ratio (16/18) of isotopic frequencies. [b] Annealing behavior: a denotes presence on deposition and +, −, or 0 indicates the direction of growth in two successive annealings; b denotes appearance on the first annealing and +, −, or 0 indicates changes on second annealing; (+ or −) indicates changes on photolysis; * indicates an increase with CCl_4 on deposition; ** indicates a decrease with CCl_4 on deposition.

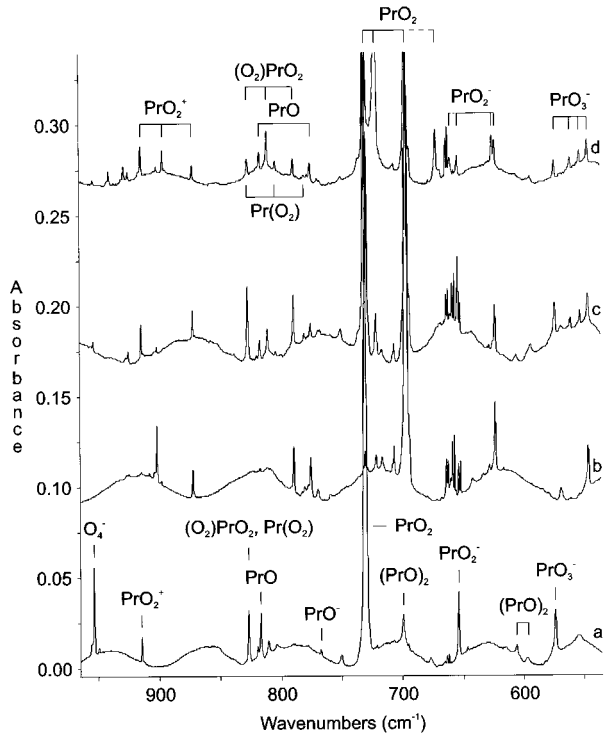

Figure 2. Infrared spectra in the 965−535 cm^{-1} region for low-power laser-ablated praseodymium atoms co-deposited with (a) 1% $^{16}O_2$/Ar after 1 h deposition, (b) 1% $^{18}O_2$/Ar after 1 h deposition, (c) 2% ($^{16}O_2$ + $^{18}O_2$)/Ar after 1 h deposition, (d) 2% ($^{16}O_2$ + $^{16}O^{18}O$ + $^{18}O_2$)/Ar after 1.25 h deposition.

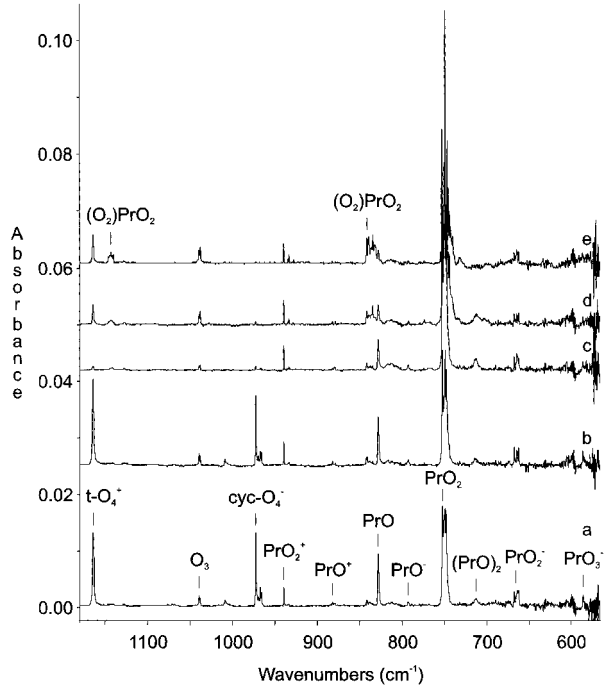

Figure 3. Infrared spectra in the 1180−565 cm^{-1} region for laser-ablated praseodymium atoms co-deposited with 0.2% $^{16}O_2$/Ne after (a) 40 min deposition, (b) annealing to 6 K, (c) 10 min Hg-arc photolysis, (d) annealing to 9 K, (e) annealing to 12 K.

NdO Species. Three forms of NdO are observed, NdO^+, NdO, and NdO^- (Figure 4). The cation absorbs at 848.3 (804.4) cm^{-1}, decreases with annealing, increases with photolysis, and also increases with CCl_4 dopant (Table 3). The cation has an oxygen isotopic ratio of 1.0537, in good agreement with 1.0542, the harmonic ratio for NdO. The neutral NdO fundamental is

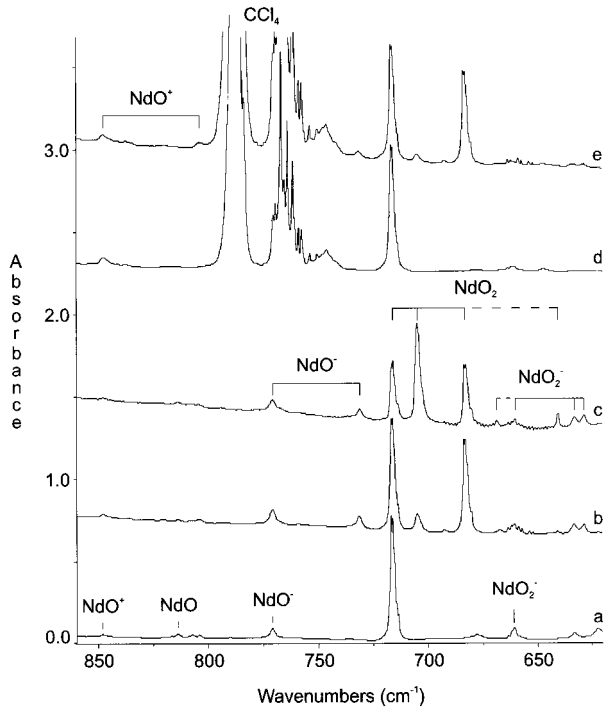

Figure 4. Infrared spectra in the 860−620 cm^{-1} region for laser-ablated neodymium atoms co-deposited with (a) 1% $^{16}O_2$/Ar after 1 h deposition, (b) 2% ($^{16}O_2$ + $^{18}O_2$)/Ar after 1 h deposition, (c) 1% ($^{16}O_2$ + $^{16}O^{18}O$ + $^{18}O_2$)/Ar after 3 h deposition, (d) 1% $^{16}O_2$/0.1% CCl_4/Ar after 1 h deposition; (e) 1.5% ($^{16}O_2$ + $^{18}O_2$)/0.15% CCl_4/Ar after 1 h deposition.

observed at 814.2 (771.9) cm^{-1}, in agreement with a previous report at 813.9 cm^{-1}.[20] This molecule also appears as an impurity in nitride and hydride systems studied in this laboratory and as a product in NO systems. The neutral molecule provides a weaker absorption than the two ions in laser ablation experiments, whereas in thermal oxide experiments, neutral NdO absorbed strongly and the ion bands were not reported.[20] The cation absorbs at 848.3 (804.4) cm^{-1} in the laser ablation experiments and the anion at 771.0 (731.4) cm^{-1} (Figure 4). Unlike many anions, NdO^- is not bleached by UV photolysis but rather increases, which suggests a high electron affinity; it is, however, significantly inhibited by CCl_4 dopant in the reaction mixture, supporting the anion assignment.

Like the praseodymium oxide system, both ions and the neutral are observed for neodymium oxides in neon. The NdO^+ cation, found at 878.4 (833.9) cm^{-1} in solid neon, is 30 cm^{-1} blue-shifted from its argon position, the NdO^- anion at 789.9 (749.3) cm^{-1} is blue-shifted by 19 cm^{-1}, and the neutral NdO at 825.1 (783.0) cm^{-1} is blue-shifted by 11 cm^{-1}.

SmO Species. SmO, SmO^+, and SmO^- have all been observed in argon matrices, and the vibrational fundamentals of the ions are reported here for the first time (Table 4 and Figure 5). SmO is observed at 807.4 (765.8) cm^{-1} and absorbs weakly upon deposition of Sm and O_2 into argon matrices, although it was a dominant product in previous thermal effusion experiments.[20] SmO^+ absorbs at 840.0 (796.9) cm^{-1} and SmO^- at 770.2 (730.5) cm^{-1}, with respective oxygen isotopic ratios of 1.0541 and 1.0543, in close agreement with the neutral isotopic ratio of 1.0543 and the harmonic ratio of 1.0545.

Upon deposition, the neutral species has a relatively low intensity, the anion is sharp and absorbs more strongly, and the cation is not observed. Successive photolysis with a tungsten lamp and glass filters revealed a 5% increase in the anion intensity with $\lambda > 850$ nm and again with $\lambda > 700$ nm;

TABLE 3: Product Absorptions (cm^{-1}) Observed for Laser-Ablated Nd Atoms with O_2 in Solid Argon and Neon

$^{16}O_2$	$^{18}O_2$	$^{16}O_2 + {}^{18}O_2$	$^{16}O_2 + {}^{16}O^{18}O + {}^{18}O_2$	$R(16/18)$[a]	anneal[b]	identity
			In Argon			
1555	1466			1.061	b+	$(OO)Nd_x$
1375.5	(1305)	1375.5, (1305)	1375.2, 1342.2, (1305)	1.054	a−0	NdO_2, $\nu_1 + \nu_3$
1121.2	1058.1	1121.1, 1083.7, 1058.0		1.0596	a++(−)**	$(O_2)_2NdO_2$
1113.4	1048.3	1113.4, 1048.3	1113.6, 1083.1, 1048.3	1.0621	a++(−)**	$(O_2)NdO_2$
1103.4	1041.7	1103.4, 1079.2, 1041.7		1.0592	a++(−)**	$(O_2)_2NdO_2$ site
869.2	829.3	869.2, 829.3	869.0, 851.4, 829.3	1.0481	a++(−)*	NdO_2^+, ν_3
848.3	804.4	848.2, 804.3	848.1, 804.5	1.0546	a− −(+)*	NdO^+
814.2	771.9	814.2, - - -	814.0, - - -	1.0544	a0−(−)**	NdO
796					b+	$Nd^+O_3^-$
771.0	731.4	771.0, 731.4	771.0, 731.2	1.0541	a+ −(+)**	NdO^-
716.9	683.5	716.6, 683.6	716.9, 704.9, 683.5	1.0489	a+ −(+)	NdO_2, ν_3
713.3	680.1	713.4, 680.1	713.7, 701, 679.8	1.0488	a++	$(O_2)NdO_2$, ν_3
		667.4	667.4	1.0536	a+ −(+)**	$^{16}ONd^{18}O^-$, ν_1
			640.5		a− −(+)	$^{16}ONd^{18}O$, ν_1
660.6	628.3	660.6, 633.0, 628.3	660.4, 632.9, 628.4	1.0514	a+ −(+)**	NdO_2^-, ν_3
632.9	603.6			1.0485	a− −**	?
621.6	587.2			1.0586	a− −**	?
608.5	577.3			1.0540	a− −**	?
600.0	568.4	599.9, 586.8, 568.5	599.8, 586.4, 568.7	1.0556	a+ −(+)**	$(NdO)_2$
525.0	497.5	525.0, 497.5		1.0553	a− −(−)**	?
465.6		465.5, 442.7		1.0515	a0−(−)**	?
			In Neon			
1554.6	1466.7			1.0599	a+0	$(OO)Nd_x$
1320.1	1251.9			1.0545	a− +(−)	cyc-O_4^+
1164.3	1098.7			1.0597	a-+(−)	trans-O_4^+
1009.3	954.1			1.0578	a− −(−)	?
983.8	929.9			1.0580	a− −(−)	?
973.0	919.6			1.0581	a− −(−)	cyc-O_4^-
967.6	914.4			1.0582	a− −(−)	cyc-O_4^- site
966.2	913.2			1.0580	a− −(−)	cyc-O_4^- site
894.5	853.5			1.0480	a− −(−)	NdO_2^+, ν_3
893.5	852.4			1.0482	a− −(−)	NdO_2^+, ν_3 site
892.4	851.2			1.0484	a− −(−)	NdO_2^+, ν_3 site
878.4	833.9			1.0534	a− −(+)	NdO^+
825.1	783.0			1.0538	a− −(−)	NdO
789.9	749.3			1.0542	a++(−)	NdO^-
737.6	703.5			1.0485	a− −(+)	NdO_2, ν_3
732.4	698.7			1.0482	a0−	$(OO)_xNdO_2$, ν_3
729.0	695.4			1.0483	a++(−)	$(OO)_xNdO_2$, ν_3
638.3	609.2			1.0478	a+ −(−)	?

[a] Ratio (16/18) of isotopic frequencies, [b] Annealing behavior: a denotes presence on deposition and +, −, or 0 indicates the direction of growth in two successive annealings; b denotes appearance on the first annealing and +, −, or 0 indicates changes on second annealing; (+ or −) indicates changes on photolysis; * indicates an increase with CCl_4 on deposition; ** indicates a decrease with CCl_4 on deposition.

continuing with $\lambda > 590$ nm, SmO decreased in intensity by 60% and SmO^- gained 30%. Further photolysis using the full tungsten lamp radiation completely destroyed the neutral monoxide, while increasing the anion (Figure 5). The cation did not appear until after Hg arc photolysis, which decreased the anion and created the cation. In experiments doped with CCl_4, the cation is present upon deposition; both the neutral and the anion yields are lower, and UV photolysis gives an even greater cation absorbance. Hence, SmO (IE = 5.5 ± 0.1 eV)[34] is photoionized in the matrix by the strong Hg arc with the assistance of a 0.5 eV matrix solvent stabilization of the cation. Here, CCl_4 serves to capture the ejected electron, helping to preserve the isolated SmO^+ cation.

EuO Species. The EuO^- anion is not observed, but the EuO neutral absorbs at 667.8 (633.5) cm^{-1} and the EuO^+ cation at 756.9 (718.2) cm^{-1}. Both show a doublet of isotopic peaks in the scrambled $^{16}O_2 + {}^{16}O^{18}O + {}^{18}O_2$ samples and have oxygen isotopic ratios in reasonable agreement with the harmonic ratio of 1.0545 (Table 5). Hg arc photolysis achieves ionization of the neutral EuO, demonstrated spectroscopically by an increase in the EuO^+ cation absorption concurrent with a decrease in the EuO neutral intensity.

Except for EuO^+, the cations of the lanthanide monoxides in this study absorb 30−40 cm^{-1} higher than the neutral molecules; EuO^+ is 89.1 cm^{-1} higher than its neutral counterpart. The EuO species is also the only monoxide in the first half of the lanthanide series for which an anion is not observed. (The second part of this study[62] shows that these statements are also true for YbO.) The peculiarities of EuO (YbO) are due to the difference in the ground electronic state of this monoxide from the ground electronic states of the other lanthanide monoxides. The neutral EuO (YbO) molecule has a half-filled (full) metal 4f shell with no other nonbonding electrons on the metal; other lanthanide monoxides have one nonbonding σ electron on the metal with the remainder in the f-shell.[18,24,28] Therefore, ionization of EuO (YbO) occurs from the metal f-shell, whereas ionization of other lanthanide monoxides occurs from the nonbonding σ molecular orbital. Because the 4f electrons are radially smaller than the bond length, but the radius of the nonbonding σ orbital exceeds the bond length,[28] removal of an f-electron causes a greater change in the positive charge on the metal center perceived by the O^{2-} ligand than removal of the σ electron, which in turn results in a larger change in the vibrational frequency of the molecule. The stability of the half-

TABLE 4: Product Absorptions (cm^{-1}) Observed for Laser-Ablated Sm Atoms with O_2 in Solid Argon at 10 K

$^{16}O_2$	$^{18}O_2$	$^{16}O_2 + {}^{18}O_2$	$^{16}O_2 + {}^{16}O^{18}O + {}^{18}O_2$	$R(16/18)^a$	anneal[b]	identity
1552.2	1464.6	1552, 1464	1552, 1508, 1464	1.0598	b+	$(OO)Sm_x$
1243.8	1180.3	1243.6, 1180.3	1243.9, 1216.4, 1180.2	1.0538	a+ −(+)	SmO_2, $\nu_1 + \nu_3$ site
1242.4	1178.8	1242.2, 1178.8	1242.3, 1215.4, 1178.9	1.0540	a+ −(+)	SmO_2, $\nu_1 + \nu_3$
1114	1052	1114, 1052	1114, 1083, 1052	1.059	a++	$(O_2)SmO_2$
840.0	796.9	840.0, 796.9	840.0, 796.9	1.0541	c−*	SmO^+
807.4	765.8	807.4, 765.8	807.4, 765.8	1.0543	a0−(−)**	SmO
795	751	795, 786, 761, 752	795, 785, 776, 770, 761, 752	1.059	b+	$Sm^+O_3^-$
770.2	730.5	770.0, 730.3	770.2, 730.5	1.0543	a+ −(+)**	SmO^-
676.4	640.6	676.5, - - -	676.5, - - -, - - -	1.0559	a− −(−)**	SmO_2^-, ν_1
675.7	640.1			1.0556	a− −(−)**	SmO_2^-, ν_1 site
644.4	614.7	644.3, 614.5	644.5, 635.3, 614.9	1.0483	a+ −(+)	SmO_2, ν_3 site
643.2	613.3	643.1, 613.3	643.2, 634.0, 613.3	1.0488	a+ −(+)	SmO_2, ν_3
642.5	612.6	642.4, 612.5	642.5, 633.6, 612.7	1.0488	a+ −(+)	SmO_2, ν_3 site
639.8	609.9	640.3, 610.5	640.3, 631.1, 610.1	1.0490	a++	$(O_2)SmO_2$
			584.7		a+ −(+)	SmO_2, ν_1
576.4	548.3	576.4, 548.2	576.5, 559.8, 548.4	1.0512	a− −(−)**	SmO_2^-, ν_3 site
575.5	547.2	575.5, 547.2	575.5, 558.8, 547.2	1.0517	a− −(−)**	SmO_2^-, ν_3
564.4	535.0	564.1, 552.8, 535.1	564.2, 553.1, 535.3	1.0550	c+	$(SmO)_2$
422.6					c+	$(SmO)_2$

[a] Ratio (16/18) of isotopic frequencies, [b] Annealing behavior: a denotes presence on deposition and +, −, or 0 indicates the direction of growth in two successive annealings; b denotes appearance on the first annealing and +, −, or 0 indicates changes on second annealing; (+ or −) indicates changes on photolysis; c indicates appearance on photolysis; * indicates an increase with CCl_4 on deposition; ** indicates a decrease with CCl_4 on deposition

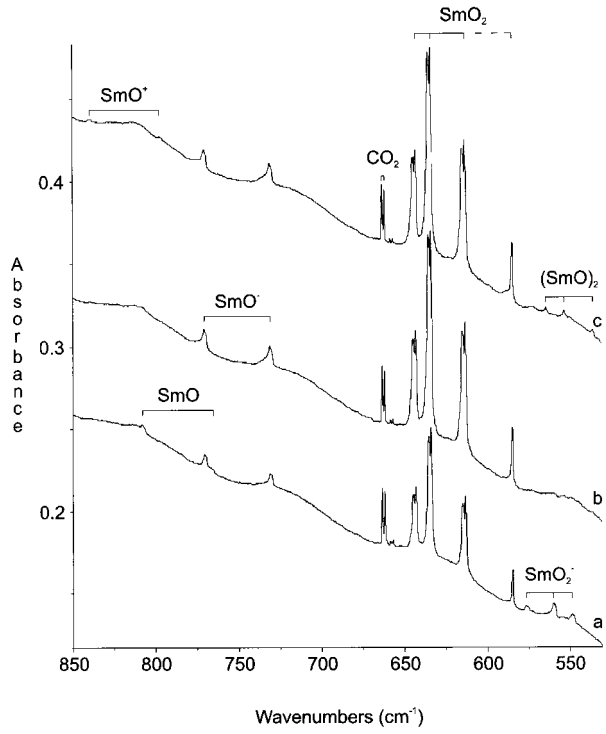

Figure 5. Infrared spectra in the 850−530 cm^{-1} region for low-power laser-ablated samarium atoms co-deposited with 2% ($^{16}O_2 + {}^{16}O^{18}O + {}^{18}O_2$)/Ar (a) after 1 h 15 min deposition, (b) after 15 min photolysis with the W lamp, (c) after 15 min photolysis with the Hg arc lamp.

filled (full) metal 4f shell also decreases the electron affinity of neutral EuO (YbO), accounting for the lack of an anion for this molecule.

GdO Species. GdO neutral and its two ions, GdO^+ and GdO^-, were all observed upon deposition of laser-ablated Gd atoms, cations, and electrons into an argon reaction mixture containing 1% O_2 (Figure 6). The isotopic ratios of the neutral, cation, and anion, 1.0542, 1.0543, and 1.0545, respectively, all agree well with the harmonic ratio of 1.0547, considering the effect of anharmonicity in the observed vibrations. Of the trio, GdO neutral, absorbing at 812.7 (770.9) cm^{-1}, and GdO^-, absorbing at 772.2 (732.3) cm^{-1}, are observed to be of comparable intensity upon deposition, while GdO^+ cation absorbs less intensely at 844.8 (801.3) cm^{-1}. Photolysis with the tungsten lamp increased the anion at the expense of the neutral but did not affect the cationic species. Hg arc photolysis decreased all three species if done prior to annealing but increased the GdO^+ cation after annealing. Addition of CCl_4 to the reaction mixture effectively reverses this situation, increasing GdO^+ considerably with respect to the neutral (Figure 6 and Table 6). In the $^{18}O_2$ spectrum with CCl_4, $Gd^{18}O^-$ is decreased with respect to $Gd^{18}O^+$, but the neutral is masked by CCl_4 absorptions.

Dioxides. The neutral dioxide and anion products are observed in all six of the lanthanide oxygen systems reported here, and two gave the cation. The observed anions of the lanthanide dioxides invariably absorb at lower frequencies than the neutrals, while the cations are higher in frequency, following the pattern set by the ions of the monoxides (Figure 2). Upon annealing, the neutral dioxide molecules ligate O_2, forming a side-bound complex, which provides a shifted frequency for the ν_3 absorption of OLnO, as seen in Tables 1−6, and an additional absorption in the 1100 cm^{-1} region corresponding to the O−O stretch of the side-bound complex. Neodymium and praseodymium dioxides trapped in neon matrices include PrO_2, PrO_2^+, PrO_2^-, NdO_2, and NdO_2^+. Like the monoxides, the cations of the dioxides experience a larger blue shift than the neutrals from an argon to a neon host.

OCeO Species. Neutral CeO_2 has been previously observed in argon matrices, and its fundamentals in this study have been measured at 736.7 (701.7) cm^{-1} for the ν_3 stretch and 757.3 (715.6) cm^{-1} for the ν_1 stretch, in agreement with previous authors.[21] The $\nu_1 + \nu_3$ combination has also been observed at 1489.5 (1413.2) cm^{-1}. The sum of the observed ν_1 and ν_3 fundamentals is 1494.0 (1417.3) cm^{-1}, 4.5 (4.1) cm^{-1} greater than the combination band owing to anharmonicity. The oxygen isotopic ratio for this absorption is 1.0540, near the average of the ν_1 and ν_3 isotopic ratios.

The ν_3 fundamental of the $OCeO^-$ anion is observed at 662.0 (630.6) cm^{-1} and the ν_1 mode at 712.0 (672.9) cm^{-1} (Figure 1). The experimentally observed oxygen isotopic ratios for these bands are similar to those tabulated for the neutral molecule, leading to the conclusion that both are bent at about 140°; previous estimates have placed the bond angle of the neutral at

TABLE 5: Product Absorptions (cm^{-1}) Observed for Laser-Ablated Eu Atoms with O_2 in Solid Argon at 10 K

$^{16}O_2$	$^{18}O_2$	$^{16}O_2 + {}^{18}O_2$	$^{16}O_2 + {}^{16}O^{18}O + {}^{18}O_2$	$R(16/18)^a$	anneal[b]	identity
1552.2	1464.5	1551.9, 1464.3	1552.0, 1508.7, 1464.3	1.0599	b+	$(OO)Eu_x$
1133.3	1075.8	1133.3, 1075.8	1133.3, 1075.8	1.0534	a+ −(+)	?
1131.4	1074.0	1131.5, 1074.3	1131.6, 1074.2	1.0534	a+ −(+)	?
1110.0	1047.8			1.0594	a++(+)	$(O_2)EuO_2$
1082.6	1021.9	1082.8, 1022.1		1.0594	a++(−)	$(O_2)EuO_2$
797	753	797, 788, 763, 753	797, 788, 778, 772, 763, 753	1.058	b+	$Eu^+O_3^-$
756.9	718.2	757.1, 718.4	757.3, 718.2	1.0539	a+ −(+)*	EuO^+
680.3	644.3	680.4, 644.4	680.3, 665.2, 644.5	1.0559	a+0(+)	?
667.8	633.5	667.8, 633.4	667.8, 633.5	1.0541	a+ −(−)	EuO
661.0	625.6	661.0, 625.6	- - -, 645.8, 625.7	1.0566	a+ −(−)**	EuO_2^-, ν_1
622.8	590.3			1.0551	a− −(+)	EuO_2, ν_3
607.9	576.0	607, 576	608, 593, 578	1.0554	a+ −(+)	$(O_2)EuO_2$, ν_3 site
602.5	571.3	602.5, 571.5	602.4, 587.7, 571.6	1.0546	b+(−)	$(O_2)EuO_2$, ν_3
571.1	544.7	571.2, 544.7	571.2, 544.6	1.0485	a+ −(+)	?
560.8	533.5	560.8, 533.5	560.8, 544.7, 533.7	1.0512	a+ −(−)**	EuO_2^-, ν_3
554.4	528.5	554.3, 528.7	554.3, 528.6	1.0490	a+ −(+)	?
530.5	503.4	530.3, 503.3	530.3, 517.5, 503.2	1.0538	a− −(+)	$(EuO)_2$
529.2	502.1	529.2, 502.1	529.2, 516.4, 502.1	1.0540	a− −(+)	$(EuO)_2$
491.3	467.3	491.3, 467.2	491.0, 473.4, 467.5	1.0514	a+ −(+)*	?
473.5	450.3			1.0515	a− −(+)**	?
444.6	422.0	444.7, 421.8	444.7, 429.8, 422.1	1.0536	a− −(+)	$(EuO)_2$
442.7	420.0	442.8, 420.0	442.8, 428.7, 420.2	1.0540	a− −(+)	$(EuO)_2$

[a] Ratio (16/18) of isotopic frequencies, [b] Annealing behavior: a denotes presence on deposition and +, −, or 0 indicates the direction of growth in two successive annealings; b denotes appearance on the first annealing and +, −, or 0 indicates changes on second annealing; (+ or −) indicates changes on photolysis; * indicates an increase with CCl_4 on deposition; ** indicates a decrease with CCl_4 on deposition.

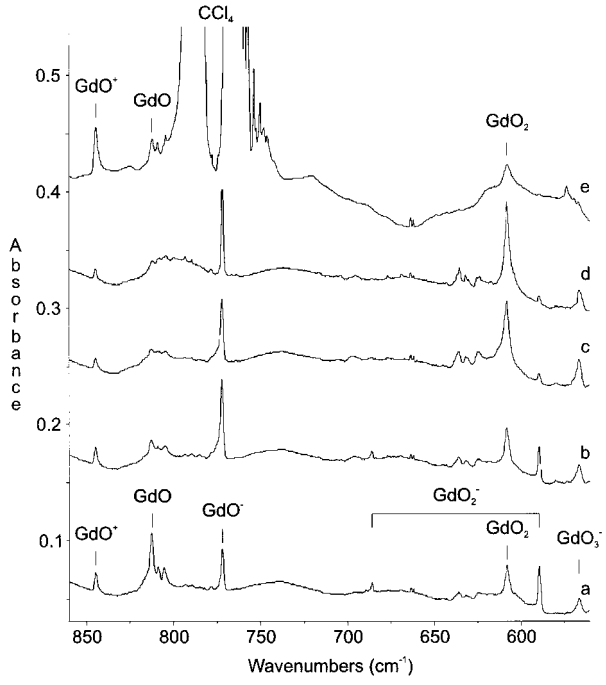

Figure 6. Infrared spectra in the 860−560 cm^{-1} region for low-power laser-ablated gadolinium atoms co-deposited with (a) 1% $^{16}O_2$/Ar after 1 h deposition, (b) 1% $^{16}O_2$/Ar after 10 min photolysis with the tungsten lamp, (c) 1% $^{16}O_2$/Ar after 20 min photolysis with the Hg arc lamp, (d) 1% $^{16}O_2$/Ar after annealing to 25 K, (e) 1% $^{16}O_2$/0.1% CCl_4/Ar after 1.5 h deposition.

146°, which is within the limits of the estimate calculated from the oxygen isotopic ratio for the ν_3 stretching mode.[21,63] The $\nu_1 + \nu_3$ combination band of the dioxide anion absorbs weakly in $^{16}O_2$ ($^{18}O_2$) experiments at 1369.0 (1298.5) cm^{-1} but is too weak to observe in mixed or scrambled oxygen samples.

OPrO Species. The ν_3 fundamental of neutral PrO_2 occurs at 730.1 (696.1) cm^{-1}, and the ν_1 is not observed for this linear molecule[21] except for the isotopically substituted $^{16}OPr^{18}O$ (Figure 2). However, identification of the $\nu_1 + \nu_3$ band at 1424.4 (1351.5) cm^{-1} allows prediction of the ν_1 frequency at 696.0 (657.1) cm^{-1}. In neon these bands are observed at 1462.5 (1387.5) and 752.5 (717.5) cm^{-1}, which predicts ν_1 at 711.7 (671.7) cm^{-1}. The 14 and 22 cm^{-1} blue shifts in the stretching fundamentals from argon to neon are reasonable for OPrO.

The previously unobserved $OPrO^-$ anion absorbs sharply at 653.8 (623.2) cm^{-1} (Figure 2) and decreases with photolysis and annealing above 25 K. It has an isotopic ratio higher than the neutral molecule, predicting an angle of about 155°.[63] The ν_1 stretch of $OPrO^-$ is observed at 665.0 (628.2) cm^{-1}, but no combination band for this anion was found. Doping of the reactant mixture with CCl_4 nearly eliminated the bands due to $OPrO^-$, cementing the assignment to an anionic species. The doublet of peaks in the mixed $^{16}O_2 + {}^{18}O_2$ and the triplet of peaks in the scrambled $^{16}O_2 + {}^{16}O^{18}O + {}^{18}O_2$ samples (Figure 2) verify that exactly one O_2 molecule is involved in the formation of this dioxide, which therefore likely proceeds by direct insertion of atomic praseodymium into molecular oxygen followed by electron capture. In neon, only the ν_3 fundamental of $OPrO^-$ was observed at 667.6 (636.2) cm^{-1} (Figure 3), 13.8 (13.0) cm^{-1} blue-shifted from the argon position.

Linear $OPrO^+$ is also present in the reaction system at 914.1 (872.1) cm^{-1}; its yield relative to the neutral dioxide insertion product increases 6-fold with CCl_4 doping of reaction mixtures, strongly indicative of a cation. This cation shows a clear doublet in mixed and triplet in scrambled oxygen samples and has an oxygen isotopic ratio of 1.0482, slightly lower than the neutral ratio of 1.0488 and the harmonic ratio for the linear molecule, 1.0487. Therefore, it is proposed that the cation $OPrO^+$ is linear, unlike the CeO_2 molecule but like the neutral PrO_2 molecule, and that the anion PrO_2^- is bent, unlike the linear ONdO molecule. This geometric difference of the PrO_2 ionic species from neutral dioxides of neighboring lanthanides indicates that the electronic states of the praseodymium dioxide ions are different from those of the respective neutrals, even though the number of valence electrons is the same. Finally, $OPrO^+$ absorbs at 939.8 (896.6) cm^{-1} in solid neon, blue-shifted from the argon value by 25.7 (24.5) cm^{-1}, slightly more than the 22.4 (21.4) cm^{-1} blue shift for the PrO_2 neutral molecule.

TABLE 6: Product Absorptions (cm^{-1}) Observed for Laser-Ablated Gd Atoms with O_2 in Solid Argon at 10 K

$^{16}O_2$	$^{18}O_2$	$^{16}O_2 + {}^{18}O_2$	$^{16}O_2 + {}^{16}O^{18}O + {}^{18}O_2$	$R(16/18)^a$	anneal[b]	identity
1555	1465	1555, 1466	1554, 1510, 1466	1.061	b+	$(OO)Gd_x$
1112.7	1049.7	1112.7, 1049.8	1112.7, 1081.6, 1049.8	1.0600	a+ −(+)	$(O_2)GdO_2$
1010	955			1.0576	b+	?
844.8	801.3	844.6, 801.1	844.6, 800.9	1.0543	a− −(+)*	GdO^+
812.7	770.9	812.6, - - -	812.7, - - -	1.0542	a− −(−)**	GdO
809.0	767.2	809.1, 767.4	809.2, 767.5	1.0545	a− −(−)**	GdO site
805.6	764.3	805.9, 764.4	805.5, 764.3	1.0540	a− −(−)**	GdO site
805	761			1.058	b+	$Gd^+O_3^-$
798	753	798, 760	790, 760	1.060	b+	$Gd^+O_3^-$ site
778.4	738.2	778.4, 738.3		1.0545	a+ −(−)	GdO^- site
772.2	732.3	772.1, 732.1	772.0, 732.2	1.0545	a+ −(+)	GdO^-
685.9	649.7	685.8, - - -		1.0557	a− −(−)**	GdO_2^-, ν_1
635.5	602.9			1.0541	a− −(+)	GdO_2, ν_3
608.1	575.7	608.1, 575.8	607.9, 592.6, 576.0	1.0563	a+ −(+)	$(O_2)GdO_2$, ν_3
589.4	560.2	589.3, 560.1		1.0521	a− −(−)**	GdO_2^-, ν_3
566.1	538.7	566.1, 557.1, 548.1, 538.7	566.3, 557.1, 548.1, 538.7	1.0509	a− −(+)**	GdO_3^-
552.4	524.2			1.0538	a− −(+)	?
533.7	506.8			1.0531	a− −(−)**	?
528.7	500.9	528.7, 500.9	528.4, 500.9	1.0555	a+ −(+)**	?
516.8	490.4		516.7, 490.5	1.0538	a+ −(+)	?

[a] Ratio (16/18) of isotopic frequencies, [b] Annealing behavior: a denotes presence on deposition and +, −, or 0 indicates the direction of growth in two successive annealings; b denotes appearance on the first annealing and +, −, or 0 indicates changes on second annealing; (+ or −) indicates changes on photolysis; * indicates an increase with CCl_4 on deposition; ** indicates a decrease with CCl_4 on deposition.

ONdO species. The NdO_2 neutral, NdO_2^+ cation, and NdO_2^- anion have been observed in infrared spectra of neodymium oxides trapped in argon matrices. Although NdO_2 has been studied by mass spectrometry,[32] the vibrational frequencies have not been previously reported. The frequencies of NdO_2 were calculated (754, 256, and 716 cm^{-1}) assuming a 120° bond angle.[32] However, the infrared spectrum (Figure 4) provides evidence that ONdO is linear.

The strongest feature in the spectra of argon matrices containing neodymium oxides at 716.9 (683.5) cm^{-1} is assigned to the ν_3 stretch of ONdO. This absorption provides an isotopic doublet of peaks with mixed oxygen samples and a triplet of peaks with scrambled oxygen samples, attesting to a dioxide formed by reaction of atomic neodymium with a single oxygen molecule. The experimental oxygen isotopic ratio of 1.0489 is appropriate for a linear molecule, which has the same calculated harmonic isotopic ratio. Finally, ONdO is observed in solid neon at 737.6 (703.5) cm^{-1}, blue-shifted from the argon by 20.7 (20.0) cm^{-1}.

A weak absorption at 1375.5 (1305) cm^{-1} is assigned to the $\nu_1 + \nu_3$ combination band of ONdO. This band also exhibits isotopic doublets and triplets for mixed and scrambled oxygen samples, respectively, and tracks well with the ν_3 fundamental through photolysis and annealing cycles. The ν_1 stretch is observed only for $^{16}ONd^{18}O$ at 640.5 cm^{-1}. The sum of the ν_1 and ν_3 bands of $^{16}ONd^{18}O$ is 1345.4 cm^{-1}, only 3.2 cm^{-1} greater than the combination band observed for these stretches at 1342.2 cm^{-1}. Adding 3.2 cm^{-1} to the observed combination band for the $^{16}ONd^{16}O$ ($^{18}ONd^{18}O$) molecule to account for anharmonicity and subtracting the observed ν_3 stretch provide a good estimate of the ν_1 fundamental at 661.8 (625) cm^{-1} (ratio: 1.0589). The discovery of the ν_1 fundamental lower than the ν_3 fundamental is additional evidence that supports the linear structure for ONdO. We note that the isoelectronic OUO molecule is also linear[41] and has a higher ν_3 fundamental at 776 cm^{-1} due to relativistic effects, which strengthen the bonding in heavy elements.[42]

Following the example of OUO,[64] the cation of the isoelectronic ONdO species, NdO_2^+, has been characterized. New bands for NdO_2^+ at 869.2 (829.3) cm^{-1} in argon and 894.5 (853.5) cm^{-1} in neon are about 155 cm^{-1} higher than the neutral counterpart, similar to PrO_2^+, which was found about 190 cm^{-1} higher than PrO_2. The isotopic ratio, 1.0481, indicates that the observed stretch is the ν_3 mode of a linear $ONdO^+$ species, which is expected, since the isoelectronic OUO^+ cation is also linear,[64] as is the ONdO molecule. Mixed oxygen isotopic samples provide a doublet of peaks, but the absorptions were too weak to be observed in scrambled samples. However, given the correlation with the PrO_2^+ model, the assignment of the observed stretch to the ν_3 mode of $ONdO^+$ is secure. The argon to neon blue shift for this cation is 25.3 (24.2) cm^{-1}, similar to the shift for $OPrO^+$ and larger than the shift for neutral ONdO.

The anion, $ONdO^-$, is observed at 660.6 (628.3) cm^{-1} in spectra of laser-ablated neodymium atoms deposited into a 1% O_2/Ar mixture. This band exhibits an oxygen isotopic triplet in both mixed and scrambled oxygen experiments, suggesting formation by addition of O atoms to NdO^- or O^- to NdO, whereas the neutral is formed by direct insertion into molecular O_2. Its isotopic ratio of 1.0514 suggests that this anion is bent to roughly 120°, as opposed to the neutral and cationic species, which are linear. The ν_1 stretch is observed for the $^{16}ONd^{18}O^-$ isotope at 667.4 cm^{-1}, which is higher than the ν_3 counterpart at 632.9 cm^{-1}, supporting the conclusion that this anion is bent. Although the anion increases slightly with photolysis and annealing below 25 K, consistent with the above O atom reaction, it is decreased significantly in the presence of CCl_4, confirming its identity as an anionic species.

OSmO Species. OSmO molecules have been isolated in argon matrices both as neutrals and anions. The ν_3 fundamental of the neutral species presents the most intense feature in the spectra of samarium oxides trapped in argon at 643.2 (613.3) cm^{-1} (Figure 5). The familiar oxygen isotopic pattern identifying the fundamentals of the LnO_2 molecules is repeated here, indicating formation by direct insertion of atomic samarium into molecular oxygen. The experimental oxygen isotopic ratio is 1.0488, in accord with the harmonic ratio for the linear triatomic, 1.0493. Thus, OSmO, like ONdO and OPrO, is found to have a linear structure. In addition to the ν_3 fundamental, the $\nu_1 + \nu_3$ combination band of OSmO is observed at 1242.4 (1178.8) cm^{-1}. The ν_1 fundamental of $^{16}OSm^{18}O$ absorbs at 584.7 cm^{-1}, lower than its ν_3 counterpart at 634.0 cm^{-1}, yielding a sum of 1218.7 cm^{-1}, which is only 3.3 cm^{-1} in excess of the

combination band observed for this isotope at 1215.4 cm^{-1}. The ν_1 fundamentals of $^{16}OSm^{16}O$ and $^{18}OSm^{18}O$ can then be calculated by adding 3.3 cm^{-1} to the observed combination bands to account for anharmonicity and by subtracting the observed ν_3 absorption, arriving at values of 602.5 and 568.8 cm^{-1} for the ν_1 fundamentals of $^{16}OSm^{16}O$ and $^{18}OSm^{18}O$, respectively. (This ratio, 1.0592, is appropriate for the symmetric stretching mode of a linear molecule.) Note that like ONdO the ν_1 fundamentals are lower than the ν_3 fundamentals, consistent with a linear molecule, as evidenced by the oxygen isotopic ratio.

The ν_3 fundamental of $OSmO^-$ anion is observed in solid argon at 575.5 (547.2) cm^{-1} and exhibits an oxygen isotopic ratio of 1.0517, indicating that the anion is bent to about 120°. This band is clearly due to an anionic species because it is completely absent from experiments doped with an electron scavenger. Unlike its neodymium counterpart, the samarium dioxide anion exhibits a doublet in mixed and triplet in scrambled oxygen samples, showing that it is formed by reaction of a Sm metal atom with a single O_2 molecule followed by electron capture, not by successive addition of O and O^- atoms to the metal center, as was the case for $ONdO^-$ anion. The ν_1 stretch of the anion absorbs at 676.4 (640.6) cm^{-1} and is matrix-split in a fashion similar to the ν_3 absorption.

Experiments done with high laser power do not provide any evidence for the $OSmO^-$ anion, and the SmO neutral monoxide is barely detectable. After a neutral density filter was placed in the laser beam, the samarium dioxide anion was observed upon deposition and the monoxide neutral increased by 7 times relative to the monoxide anion. Using only 10% of the laser intensity allowed ablation of the samarium target without most of the harsh light that accompanies the ablation process. The light from the laser plume of a standard experiment is ample to detach the electron from $OSmO^-$ anions, allowing some of these free electrons to be captured by SmO neutral molecules.

The electron transfer from the dioxide anion to the monoxide neutral is demonstrated plainly in Figure 5. Deposition with low laser power yields the neutral and anion of both the monoxide and dioxide of samarium. Initial photolyses were accomplished with a tungsten lamp using a succession of long-wavelength pass filters, beginning at 850 nm and progressing through 700−590 nm and then the unfiltered tungsten lamp, and finally the unfiltered Hg arc lamp was used. With the 850 nm filter, only the monoxide anion changed, increasing by 5%. After photolysis with wavelengths longer than 700 nm, the dioxide anion experienced a 20% decrease, the dioxide neutral increased, the monoxide anion increased again by 5%, and the monoxide neutral did not experience measurable change. Photolysis with wavelengths longer than 590 nm continued this trend, but with a noticeable decrease in the monoxide neutral, and finally photolysis with the full tungsten lamp destroyed the dioxide anion and the monoxide neutral completely while enhancing both the dioxide neutral and the monoxide anion. Subsequent unfiltered Hg arc photolysis had no effect on the neutral dioxide of samarium because all of the dioxide anion had been exhausted.

OEuO Species. A weak absorption at 622.8 (590.3) cm^{-1} that increases with photolysis but decreases with annealing is assigned to the ν_3 stretch of bent EuO_2 (O−Eu−O angle near 90°). With annealing, this band red-shifts to 602.5 (571.3) cm^{-1} and intensifies to become the strongest peak in the spectrum after 35 K annealing. Precedent set by other identifications in both nitrogen and oxygen systems allows this red shift to be attributed to O_2 ligation of the EuO_2 molecule, which also often results in intensification of the observed vibrations. The mixed and scrambled isotopic components of the uncomplexed neutral could not be determined, but those of the ligated neutral dioxide absorbed prominently, presenting a doublet for the mixed $^{16}O_2 + {}^{18}O_2$ samples and a triplet for the scrambled $^{16}O_2 + {}^{16}O^{18}O + {}^{18}O_2$ samples, clearly attesting the presence of two equivalent O atoms in the observed vibration with both originating from the same O_2 subunit. Because the apex angle in this molecule is close to 90°, the interaction between the two bond vibrations should be small, but in the complexed molecule, the interaction is enhanced, allowing observation of the $^{16}OEu^{18}O$ ν_3 stretch in the $^{16}O_2 + {}^{16}O^{18}O + {}^{18}O_2$ experiment. Since Ln−O bond lengths in monoxides are about 1.8 Å, the Ln−O bonds of dioxides can be estimated to be 2.0 Å, which predicts an O−O distance of ∼2.8 Å and thus the absence of O−O bonding.

Although the experimental ratio of the observed isotopic fundamentals is reminiscent of a rhombic $(EuO)_2$ dimer, another obvious possibility for a dioxide species, this identification is rejected, since there is very good evidence for both the B_{2u} and B_{3u} modes of just such a species about 90 and 180 cm^{-1} lower, respectively, which is where the rhombic dimers are expected to absorb relative to the MO_2 species.

The $OEuO^-$ anion also exhibits a doublet in mixed experiments at 560.8 and 533.5 cm^{-1} and a triplet in scrambled experiments at 560.8, 544.7, and 533.7 cm^{-1} and so is clearly due to a dioxide species with both O atoms originating from the same O_2 molecule. Furthermore, the assigned $OEuO^-$ ν_3 fundamental decreases with annealings exceeding 25 K and with photolysis and is not present at all in spectra taken of CCl_4-doped samples, so it is very likely correctly identified as an anion. Its oxygen isotopic ratio of 1.0512 is similar to ratios of previously assigned lanthanide dioxides and, neglecting anharmonicity, predicts this anion to be bent at about 130°.[63] The ν_1 fundamental is also observed weakly at 661.0 (625.6) cm^{-1}. It too shows a doublet in mixed and a triplet in scrambled isotopic oxygen experiments, and its $^{16}O/^{18}O$ ratio of 1.0566 is appropriate for this mode.

OGdO Species. Like EuO_2, GdO_2 absorbs in the same region at 635.5 (602.9) cm^{-1}, providing an oxygen isotopic ratio of 1.0541, appropriate for a bent dioxide with an apex angle of about 97°.[63] Although congestion and broadening of peaks with mixed and scrambled isotopic samples precludes observation of the uncomplexed neutral molecule, the doublet in mixed oxygen and triplet in scrambled oxygen experiments found for the ligated molecule, which increases on annealing, identifies this species as a dioxide formed by reaction of atomic metal with a single dioxygen unit.

The ν_3 fundamental of the anion occurs at 589.4 (560.2) cm^{-1} and the ν_1 mode at 685.9 (649.7) cm^{-1}. These bands are favored by deposition with low laser power and decrease both with photolysis and annealing of samples, maintaining constant relative intensities. Introduction of trace quantities of CCl_4 into the samples eliminates both absorptions completely, further linking them to each other and identifying the molecule as an anion. In mixed $^{16}O_2 + {}^{18}O_2$ samples, both isotopic ν_3 absorptions are observed with no obvious intermediate peak. The isotopic ratio of the observed ν_3 fundamentals allows a 120° estimate of the bond angle for the dioxide anion, $OGdO^-$.

Trioxide Anions. LnO_3^- was observed in only two instances for the early lanthanide series. The trioxide anion, with either C_{3v} or D_{3h} symmetry, has also been observed for V, Nb, and Ta metals and confirmed by density functional calculations.[65] The neutral trioxide has not been observed for any of the

lanthanide metals, although uranium, an actinide, formed a "T"-shaped neutral trioxide.[41,64]

PrO_3^-. The PrO_3^- anion exhibits one absorption in $^{16}O_2$ ($^{18}O_2$) experiments at 573.9 (546.0) cm^{-1} due to the doubly degenerate (e) mode of the D_{3h} (or C_{3v}) molecular anion. In mixed and scrambled isotopic oxygen experiments, a quartet of peaks is observed (Figure 2) with the middle two peaks about half the intensity of the outside peaks. The middle peaks are each due to one of the a_1 modes of the $Pr^{16}O_2{}^{18}O^-$ and $Pr^{18}O_2{}^{16}O^-$ anions, which descend from the e modes of the pure isotopic molecules when oxygen isotopic substitution lowers the molecular symmetry. The other mode that descends from the e mode remains in a position so close to that of the e mode of the isotopically pure molecules that the two cannot be resolved when both isotopically pure and isotopically mixed molecules are present. This explains the buildup of intensity in the outside peaks, which contain an e mode and a b_1 mode, relative to the inside peaks, which contain only an a_1 mode, resulting in an overall intensity distribution among the four peaks that approximates a 2:1:1:2 pattern.[66]

This absorption is completely absent from experiments doped with CCl_4, cementing its identity as an anion, and the observed mechanics are certainly consistent with a C_{3v} or D_{3h} trioxide species. V, Nb, and Ta, like Pr, have five valence electrons and also form the trioxide anion. The experimental oxygen isotopic ratio of the trioxide anion is 1.0511, which is higher than the ratio of the ν_3 fundamental of the praseodymium dioxide anion (1.0491) for 155° but much lower than the ratio (1.0541) for 90°. Therefore, the PrO_3^- anion probably has a planar D_{3h} rather than a pyramidal C_{3v} structure.

The formation mechanism could involve addition of O to PrO_2^- or O^- to PrO_2, alternatively, O_2^- may react with PrO, or PrO^- with O_2. In some experiments, PrO_3^- experienced a small increase with UV photolysis, while PrO_2^- and O_3 decreased by a similar margin, suggesting that the $O + PrO_2^-$ mechanism is at least partially responsible for formation of PrO_3^-. This behavior is more prominent for the GdO_3^- molecule.

GdO_3^-. A single absorption at 566.1 (538.7) cm^{-1} is assigned to the GdO_3^- anion. Typical of this type of molecule, a quartet of peaks, with positions at 566.1, 557.1, 548.1, and 538.7 cm^{-1}, is observed in both mechanically mixed and scrambled oxygen samples. Unlike the PrO_3^- anion, the middle peaks of the quartet are 2−4 times as intense as the outside peaks. This follows the mechanical model of a nondegenerate mode of three equivalent O atoms, which could arise from a distorted structure with lower symmetry (C_{2v}). Photolysis yields an increase in the GdO_3^- anion concomitant with a decrease in the GdO_2^- anion. This is not due to electron capture by GdO_3, as the neutral molecule was not found in the spectra, but rather due to photodissociation of ozone, which also decreased with UV photolysis, and reaction of the O atom with GdO_2^-, producing the trioxide anion, GdO_3^-.

$(LnO)_2$ Rings. A dimetal dioxide ring of D_{2h} or C_{2v} symmetry has been observed in five of the six lanthanide systems. The ring forms both through dimerization of the monoxide molecule and through addition of a second metal atom to a metal dioxide or metal dioxygen complex.[67] This ring absorbs in a lower frequency region of the spectrum than the dioxide insertion product. These absorptions are often diminished upon the addition of CCl_4 to the sample, raising the possibility of assignment to anionic species. However, the presence of CCl_4 does inhibit formation of larger molecules as well as anions, and similar species were observed in thermal experiments,[23] where anions are unlikely. Higher laser power favors formation of these molecules more than the metal monoxides and metal dioxides, supporting assignment to a higher metal species.

$(CeO)_2$. Two absorptions in $^{16}O_2$ ($^{18}O_2$) spectra with laser-ablated cerium atoms at 575.0 (547.1) and 483.6 (459.5) cm^{-1} track with each other through photolysis and annealing cycles (Figure 1). Experiments done with mechanically mixed $^{16}O_2 + {}^{18}O_2$ and statistically scrambled $^{16}O_2 + {}^{16}O^{18}O + {}^{18}O_2$ samples both show isotopic triplets for the two peaks with central components at 561.5 and 470.1 cm^{-1}. In the mixed isotopic experiment the isotopic peaks closely approximate a 1:1:1 intensity ratio, while in the scrambled isotopic experiment, the isotopic intensity ratio is 1:2:1, indicating that both dimerization and secondary reaction mechanisms are active in the formation of this species. The $^{16}O/^{18}O$ isotopic ratios for the two peaks are 1.0510 and 1.0524, just below the CeO ratio of 1.0537, which suggests that this ring is puckered, as the isotopic ratios of a planar rhombic ring should be nearly the same as those for the monoxide.

$(PrO)_2$. Two modes of this molecule are observed, the higher mode at 699.2 (663.0) cm^{-1} and the lower one split by an apparent Fermi resonance into two absorptions at 605.8 (568.4) and 593.7 (560.6) cm^{-1}. With annealing of argon matrices, $(PrO)_2$ ligates O_2 and is red-shifted in the spectra. The complexed absorptions, occurring at 679.1 (646.1) and 596.1 (567.0) cm^{-1}, respectively, do not exhibit Fermi resonance and provide respective isotopic ratios of 1.0532 and 1.0513, which indicates that this molecule, like $(CeO)_2$, is a puckered ring. Mixed oxygen samples provide a 1:1 isotopic doublet of peaks, while scrambled samples provide the 1:2:1 triplet, which illustrates that $(PrO)_2$ is formed by addition of atomic Pr to a dioxide or dioxygen complex.

$(NdO)_2$. The cyclic $(NdO)_2$ molecule is observed at 600.0 (568.4) cm^{-1} in solid argon and, like $(CeO)_2$, shows a triplet in both mixed and scrambled oxygen experiments. The isotopic intensity ratio in the mixed samples approximates 1:1:1 but is closer to 1:2:1 in scrambled oxygen isotopic experiments, illustrating the activity of both dimerization and secondary reaction mechanisms. The oxygen isotopic ratio (1.0556) is slightly above NdO (1.0544) and suggests that this molecule is nonplanar.

$(SmO)_2$. In the $^{16}O_2$ samples, two modes of $(SmO)_2$ were observed at 564.4 (535.0) and 422.6 cm^{-1}, respectively. Although both bands are sharp, the lower mode at 422.6 cm^{-1} is too close to the end of the spectrum for any isotopic counterparts to be determined. However, the clarity of the $^{16}O_2$ spectra in this region is such that the association of the two peaks is obvious, and the higher mode can be readily traced isotopically. This molecule is formed by photolysis of the reaction system and therefore does not absorb upon deposition. It exhibits the now familiar 1:1:1 and 1:2:1 triplets with mixed and scrambled oxygen isotopic samples. The oxygen isotopic ratio (1.0550) suggests that this molecule is nonplanar.

$(EuO)_2$. Strong absorptions in the $^{16}O_2$ ($^{18}O_2$) samples at 530.5 (503.4) and 444.6 (422.0) cm^{-1} are attributed to the B_{2u} and B_{3u} fundamentals of $(EuO)_2$. Mixed oxygen isotopic samples provide doublets of peaks, while scrambled samples yield a very definite 1:2:1 isotopic intensity pattern for two triplets. It is therefore concluded that this molecule forms only through a dioxide or dioxygen complex of europium and not through the dimerization route followed in previous cases. Because the isotopic frequency ratios of both peaks match the monoxide ratio, the $(EuO)_2$ molecule probably has the rhombic (D_{2h}) structure.

$Ln(O_2)$. In addition to the inserted dioxides, dioxygen complexes of the lanthanide metals have been isolated in argon matrices for the Ce and Pr systems in the 800 cm^{-1} region. These species provide a doublet in mixed oxygen and triplet in isotopically scrambled oxygen samples. The oxygen isotopic ratio of the Pr band is estimated at 1.060, since the $^{16}O_2$ counterpart is obscured, and that of the Ce band is 1.0579, slightly lower than a pure O−O isotopic stretching ratio. The isotopic pattern indicates vibration of two O atoms originating from the same O_2 molecule, and the isotopic ratio of the Ce counterpart, as well as the peak position, is suggestive of a peroxo-type molecule. Therefore, these vibrations are assigned to the O−O stretches of the $Ce(O_2)$ and $Pr(O_2)$ peroxo rings, analogous to $Fe(O_2)$.[45]

$(O_2)LnO_2$ and $(O_2)_2LnO_2$ Complexes. Upon annealing of rare gas matrices, the most intense absorption of OLnO experiences a small but discernible red shift for OCeO, ONdO, and OSmO, a larger red shift of 20−30 cm^{-1} for OEuO and OGdO, and a sizable blue shift of about 100 cm^{-1} for OPrO. This shift occurs when O_2 complexes the OLnO molecule in a side-bound fashion. The aberration in the case of OPrO is attributed to its ease of ionization, exemplified by the observation of the $OPrO^+$ species. In this instance, OPrO attains a partial positive charge, balanced by a partial negative charge on the O_2 ligand, which causes a blue shift in the frequency of the OPrO absorption to a position about midway between that of the cation and the neutral molecules. For the other lanthanide dioxides, the ligation by O_2 does not involve such a strong ionic interaction and so causes less perturbation in the position of the dioxide ν_3 fundamental. For Pr and Nd, the dioxide complexes two O_2 units in addition to the singly ligated species observed for the other metals. The O−O stretches for the doubly ligated species are observed at frequencies similar to those for the singly ligated species. Frequencies observed for the OLnO and O−O vibrations of these complexes are listed for each metal in Tables 1−6.

Metal Ozonides. Five of the six lanthanide oxide systems studied provide a peak near 795 cm^{-1} that is attributed to an O_3^- fundamental of the $Ln^+O_3^-$ species. This agrees with previous lanthanide ozonide assignments, restricted to praseodymium and samarium,[35] and the analogous alkali metal ozonide species.[36] Observation of the $Ln^+O_3^-$ species shows that the lanthanide metal atoms also have a +1 oxidation state. In the samarium and europium systems, the isotopic absorptions for the observed vibration are clear enough to observe a quartet in the oxygen isotopically mixed samples and a sextet in the isotopically scrambled oxygen samples.

Other Complexes. Metal clusters, which form when rare gas matrices containing metal atoms are annealed, weakly perturb molecular O_2, allowing it to absorb infrared radiation near 1552 cm^{-1} after annealing of samples, the absorption nearly unchanged in frequency from the Raman value observed for O_2 in argon matrices.[68] Several unidentified O−O stretching modes are also listed in the tables, notably in the Pr + O_2 system. These bands are assigned to additional molecular oxygen complexes, which cannot be positively identified from the spectral data.

Conclusions

The reaction products of laser-ablated early lanthanide metal atoms with molecular oxygen have been isolated and identified in rare gas matrices by isotopic oxygen substitution. Assignments of neutral lanthanide monoxide species concur with past identifications made from matrix isolation experiments and gas-phase values. Argon matrix vibrational fundamentals of lanthanide monoxides are 15 ± 5 cm^{-1} below the gas-phase values. The vibrational frequencies of the cations and anions of the lanthanide monoxides reported here for the first time are found to be 30−40 cm^{-1} above and 35−50 cm^{-1} below the neutral molecule values, respectively, except for EuO^+, which is 89 cm^{-1} higher than EuO.

Several new neutral lanthanide dioxides as well as six new dioxide anions and two new dioxide cations have been identified in argon matrices. In some cases, the dioxide anions are very photosensitive and can therefore be observed only if low laser power is used for ablation of the metal target to reduce photodetachment caused by the laser plume. Carbon tetrachloride has proven to be a very effective "oxidation agent" for lanthanide oxide species, clearly favoring the trapping of cations and limiting the formation of anions in argon matrices by serving as an electron trap. Added CCl_4 more effectively limits dioxide and trioxide anions than monoxide anions, which suggests that the monoxides may have even higher electron affinities.

Evidence is presented that SmO and GdO are more electrophilic than their dioxide counterparts. Notably in the SmO/SmO^-, SmO_2/SmO_2^- system, it is demonstrated that near-infrared photons cause photodetachment of an electron from SmO_2^- concurrent with trapping of the electron by SmO. This is opposite the trend for the earliest lanthanide oxides and for transition metal oxides.[58,59,69] Among other new lanthanide oxide species identified in this study are the trioxide anions, PrO_3^- and GdO_3^-. This is the first experimental evidence for pentavalent praseodymium.

Acknowledgment. We gratefully acknowledge financial support from National Science Foundation Grant CHE 97-00116 and helpful correspondence with R. W. Field.

References and Notes

(1) Eads, C. D.; Mulqueen, P.; Horrocks, W. DeW., Jr. *J. Biol. Chem.* **1984**, *259*, 9379.

(2) Eads, C. D.; Mulqueen, P.; Horrocks, W. DeW., Jr. *Biochemistry* **1985**, *24*, 1221.

(3) Molander, G. A.; Hahn, G. *J. Org. Chem.* **1986**, *51*, 2596.

(4) Gagné, M. R.; Stern, C. L.; Marks, T. J. *J. Am. Chem. Soc.* **1992**, *114*, 275.

(5) Giardello, M. A.; Yamamoto, Y.; Brard, L. *J. Am. Chem. Soc.* **1995**, *117*, 3276.

(6) Gibson, J. K. *J. Phys. Chem.* **1994**, *98*, 11321.

(7) Weber, M. J. *Lanthanide and Actinide Chemistry and Spectroscopy*; Edelstein, N. M., Ed.; ACS Symposium Series 275; American Chemical Society: Washington DC, 1980.

(8) Linton, C.; Dulick, M.; Field, R. W. *J. Mol. Spectrosc.* **1979**, *78*, 428. Linton, C.; Dulick, M.; Field, R. W.; Carette, P.; Barrow, R. F. *J. Chem. Phys.* **1981**, *74*, 189. Linton, C.; Dulick, M.; Field, R. W.; Carette, P.; Leyland, P. C.; Barrow, R. F. *J. Mol. Spectrosc.* **1983**, *102*, 441.

(9) Shenyavskaya, E. A.; Egorova, I. V.; Lupanov, V. N. *J. Mol. Spectrosc.* **1973**, *47*, 355. Dulick, M.; Field, R. W. *J. Mol. Spectrosc.* **1985**, *113*, 105.

(10) Kaledin, L. A.; Shenyavskaya, E. A.; Kovács, I. *Acta Phys. Hung.* **1983**, *54*, 189. Kaledin, L. A.; Bloch, J. C.; McCarthy, M. C.; Gurvich, L. V.; Field, R. W. *Mol. Phys.* **1994**, *83*, 881.

(11) Linton, C.; Bujin, G.; Rana, R. S.; Gray, J. A. *J. Mol. Spectrosc.* **1987**, *126*, 370.

(12) McDonald, S. A. Ph.D. Thesis, Massachusetts Institute of Technology, Cambridge, MA, 1985.

(13) Yadav, B. R.; Rai, S. B.; Rai, D. K. *J. Mol. Spectrosc.* **1981**, *89*, 1.

(14) Kulikov, A. N.; Kaledin, L. A.; Kobyliansky, A. I.; Gurvich, L. V. *Can. J. Phys.* **1984**, *62*, 1855.

(15) Linton, C.; Gaudet, D. M.; Schall, H. *J. Mol. Spectrosc.* **1986**, *115*, 58.

(16) Liu, Y. C.; Linton, C.; Schall, H.; Field, R. W. *J. Mol. Spectrosc.* **1984**, *104*, 72.

(17) Kaledin, L. A.; Shenyavskaya, E. A. *J. Mol. Spectrosc.* **1989**, *133*, 469.
(18) Linton, C.; McDonald, S.; Rice, S.; Dulick, M.; Liu, Y. C.; Field, R. W. *J. Mol. Spectrosc.* **1983**, *101*, 332. McDonald, S. A.; Rice, S.; Field, R. W.; Linton, C. *J. Chem. Phys.* **1990**, *93*, 7676.
(19) Bernard, A.; Effantin, C. *Can. J. Phys.* **1986**, *64*, 246.
(20) DeKock, R. L.; Weltner, W., Jr. *J. Phys. Chem.* **1971**, *75*, 514.
(21) Gabelnick, S. D.; Reedy, G. T.; Chasanov, M. G. *J. Chem. Phys.* **1974**, *60*, 1167.
(22) Van Zee, R. J.; Ferrante, R. F.; Zeringue, K. J.; Weltner, W., Jr. *J. Chem. Phys.* **1981**, *75*, 5297.
(23) Konnov, S. A.; Serebrennikov, L. V.; Mal'tsev, A. A. *Russ. J. Inorg. Chem.* **1982**, *27*, 367.
(24) Dulick, M.; Murad, E.; Barrow, R. F. *J. Chem. Phys.* **1986**, *85*, 385.
(25) Dolg, M.; Stoll, H. *Theor. Chim. Act.* **1989**, *75*, 369.
(26) Dolg, M.; Stoll, H.; Flad, H.; Preuss, H. *J. Chem. Phys.* **1992**, *97*, 1162.
(27) Wang, S. G.; Pan, D. K.; Schwarz, W. H. E. *J. Chem. Phys.* **1995**, *102*, 9296. Wang, S. G.; Schwarz, W. H. E. *J. Phys. Chem.* **1995**, *99*, 11687.
(28) Field, R. W. *Ber. Bunsen-Ges. Phys. Chem.* **1982**, *86*, 771. Dolg, M.; Stoll, H.; Preuss, H. *Chem. Phys. Lett.* **1990**, *174*, 208. Dolg, M.; Stoll, H.; Preuss, H. *Chem. Phys.* **1990**, *148*, 219.
(29) Liu, W.; Dolg, M.; Li, L. *J. Chem. Phys.* **1998**, *108*, 2886.
(30) Staley, H. G.; Norman, J. H. *Int. J. Mass. Spectrosc. Ion Phys.* **1969**, *2*, 35.
(31) Ackerman, R. J.; Rauh, E. G.; Thorn, R. J. *J. Chem. Phys.* **1976**, *65*, 1027.
(32) Pupp, C.; Gingerich, K. A. *J. Chem. Phys.* **1971**, *54*, 3380. Kordis, J.; Gingerich, K. A. *J. Chem. Phys.* **1977**, *66*, 483.
(33) Heinemann, C.; Cornehl, H. H.; Schröder, D.; Dolg, M.; Schwarz, H. *Inorg. Chem.* **1996**, *35*, 2463. Cornehl, H. H.; Wesendrup, R.; Diefenbach, M.; Schwarz, H. *Chem. Eur. J.* **1997**, *3*, 1083.
(34) Cockett, M. C. R.; Nyulászi, L.; Veszprémi, T.; Wright, T. G.; Dyke, J. M. *J. Electron Spectrosc. Relat. Phenom.* **1991**, *57*, 373 and references therein.
(35) Kelsall, B. J. *Diss. Abstr. Int. B* **1980**, *40*, 5694.
(36) Spiker, R. C., Jr.; Andrews, L. *J. Chem. Phys.* **1973**, *59*, 1851.
(37) Adachi, G.; Imanaka, N. *Chem. Rev.* **1998**, *98*, 1479.
(38) Koelling, D. D.; Boring, A. M.; Wood, J. H. *Solid State Commun.* **1983**, *47*, 227.
(39) Sarma, D. D.; Rao, C. N. R. *J. Electron Spectrosc. Relat. Phenom.* **1980**, *20*, 25.
(40) Kimura, S.; Arai, F.; Ikezawa, M. *J. Electron Spectrosc. Relat. Phenom.* **1996**, *78*, 135.
(41) Gabelnick, S. D.; Reedy, G. T.; Chasanov, M. G. *J. Chem. Phys.* **1973**, *58*, 4468.
(42) Pyykkö, P. *Chem. Rev.* **1988**, *88*, 563.
(43) Burkholder, T. R.; Andrews, L. *J. Chem. Phys.* **1991**, *95*, 8697.
(44) Hassanzadeh, P.; Andrews, L. *J. Phys. Chem.* **1992**, *96*, 9177.
(45) Chertihin, G. V.; Saffel, W.; Yustein, J. T.; Andrews, L.; Neurock, M.; Ricca, A.; Bauschlicher, C. W., Jr. *J. Phys. Chem.* **1996**, *100*, 5261.
(46) Andrews, L.; Bare, W. D.; Chertihin, G. V. *J. Phys. Chem. A* **1997**, *101*, 8417.
(47) Huber, K. P.; Herzberg, G. *Constants of Diatomic Molecules*; Van Nostrand Reinhold: New York, 1979.
(48) Thompson, W. E.; Jacox, M. E. *J. Chem. Phys.* **1989**, *91*, 3826. Zhou, M. F.; Hacaloglu, J.; Andrews, L. *J. Chem. Phys.*, in press.
(49) Andrews, L.; Spiker, R. C., Jr. *J. Phys. Chem.* **1972**, *76*, 3208.
(50) Chertihin, G. V.; Andrews, L. *J. Chem. Phys.* **1998**, *108*, 6404.
(51) Andrews, L.; Ault, B. S.; Grzybowaki, J. M.; Allen, R. O. *J. Chem. Phys.* **1975**, *62*, 2461.
(52) Zhou, M. F.; Andrews, L. *J. Chem. Phys.* **1998**, *109*, 10893.
(53) Zhou, M. F.; Andrews, L. *J. Am. Chem. Soc.* **1998**, *120*, 11499.
(54) Zhou, M. F.; Andrews, L. *J. Phys. Chem. A* **1998**, *102*, 10250.
(55) Zhou, M. F.; Andrews, L. *J. Chem. Phys.* **1999**, *110*, 2414.
(56) Zhou, M. F.; Andrews, L. *J. Chem. Phys.*, in press.
(57) Illenberger, E. *Ber. Bunsen-Ges. Phys. Chem.* **1982**, *86*, 252. Matejcik, S.; Kiendler, A.; Stamatovic, A.; Märk, T. D. *Int. J. Mass. Spectrom. Ion Processes* **1995**, *149/150*, 311.
(58) Polak, M. L.; Gilles, M. K.; Ho, J.; Lineberger, W. C. *J. Phys. Chem.* **1991**, *95*, 3460.
(59) Wu, H.; Wang, L.-S. *J. Chem. Phys.* **1998**, *108*, 5310.
(60) Hiraoka, K. *J. Chem. Phys.* **1988**, *89*, 3190. Celotta, R. J.; Bennett, R. A.; Hall, J. L.; Siegel, M. W.; Levine, J. *Phys. Rev. A.* **1972**, *6*, 631.
(61) Jacox, M. E. *Chem. Phys.* **1994**, *189*, 149.
(62) Willson, S. P.; Andrews, L. Manuscript (Late Ln) in preparation.
(63) Allavena, M.; Rysnik, R.; White, D.; Calder, V.; Mann, D. E. *J. Chem. Phys.* **1969**, *50*, 3399.
(64) Green, D. W.; Gabelnick, S. D.; Reedy, G. T. *J. Chem. Phys.* **1976**, *64*, 1697. Hunt, R. D.; Andrews, L *J. Chem. Phys.* **1993**, *98*, 3690.
(65) Zhou, M. F.; Andrews, L. *J. Phys. Chem. A* **1998**, *102*, 8251.
(66) Darling, J. H.; Ogden, J. S. *J. Chem. Soc., Dalton Trans.* **1972**, 2496.
(67) Chertihin, G. V.; Andrews, L.; Rosi, M.; Bauschlicher, C. W., Jr. *J. Phys. Chem. A* **1997**, *101*, 9085.
(68) Andrews, L.; Smardzewski, R. R. *J. Chem Phys.* **1973**, *58*, 2258.
(69) Fan, J.; Wang, L.-S. *J. Chem. Phys.* **1995**, *102*, 8714.